Tao *et al. Chin. J. Mech. Eng.* (2019) 32:4
https://doi.org/10.1186/s10033-019-0319-9

Chinese Journal of Mechanical Engineering

ORIGINAL ARTICLE Open Access

Influence of Cross-Sectional Flow Area of Annular Volute Casing on Transient Characteristics of Ceramic Centrifugal Pump

Yi Tao[1,2*], Shouqi Yuan[2], Jianrui Liu[2] and Fan Zhang[2]

Abstract

The annular volute is typically used in a slurry pump to reduce the collisions between solid particles and the volute tongue and to achieve a better resistance to blocking. However, only limited studies regarding annular volutes are available, and there is no systematic design method for annular volutes. In this study, the influence of volute casing cross-sectional flow area on the hydraulic loss, pressure pulsations, and radial force under varying working conditions in a centrifugal ceramic pump are discussed in detail. Experimental tests were conducted to validate the numerical results. The results indicated that, when the volute casing flow area increases, the hydraulic performance decreases marginally under the rated working conditions, but increases at the off-design points, specifically under large flow condition. However, the volute casing with a larger flow area has a wider high-efficiency region. In addition, the increase in the volute casing flow area will decrease the pressure pulsations in the volute, regardless of the working condition, and decrease the radial force on the shaft, therefore, providing an improved pump operational stability. It is anticipated that this study will be of benefit during the design of annular volutes.

Keywords: Annular volute, Centrifugal pump, Cross section, Transient characteristics, Pressure pulsation, Radial force

1 Introduction

As a critical piece of conveying equipment, a number of industries, including chemical engineering, metal smelting, mining, and environmental protection, use ceramic centrifugal pumps to pump slurry containing solid particles that could cause serious abrasion of the flow components because of their excellent resistance to erosion, abrasion, and high temperature [1–4]. To prolong the service life of the flow components of centrifugal slurry pumps, the impellers typically have thicker blades [5, 6]. However, in centrifugal pumps, the relative flow discharged from the impeller channels typically exhibits a non-uniform distribution with a jet-wake pattern, which can be attributed to the blade thickness, the boundary layer on both sides of blades, and the secondary flows inside the impeller channels [7]. The influence of blade thickness on the transient characteristics of a centrifugal ceramic pump was reported in our previous studies [8]. In addition, the amplitude of pressure fluctuations is typically a maximum close to the tongue region, where the radial gap between the impeller and volute tongue is small and, therefore, a strong interaction can take place between the jet-wake-like flow and the volute in conventional spiral volute casings [9]. However, the effect of impact wear is observed to be the greatest in the tongue region, while sliding wear is dominant in the belly region of the volute casing [10–14]. Therefore, the volute casings of centrifugal ceramic pumps are annular instead of spiral, which means that there is an identical cross-sectional flow area from cross section I to cross section VIII, as shown in Figure 1, in the flow direction. The gap between the impeller periphery and volute tongue was then increased with the advantage of decreasing the collisions of solid particles on the volute tongue [15]. A number of studies [16–18] reported that an increment in the tongue-impeller gap could reduce pressure pulsations and the overall radial force.

*Correspondence: 41642587@qq.com
[1] Wuxi Vocational Institute of Arts and Technology, Wuxi 214206, China
Full list of author information is available at the end of the article

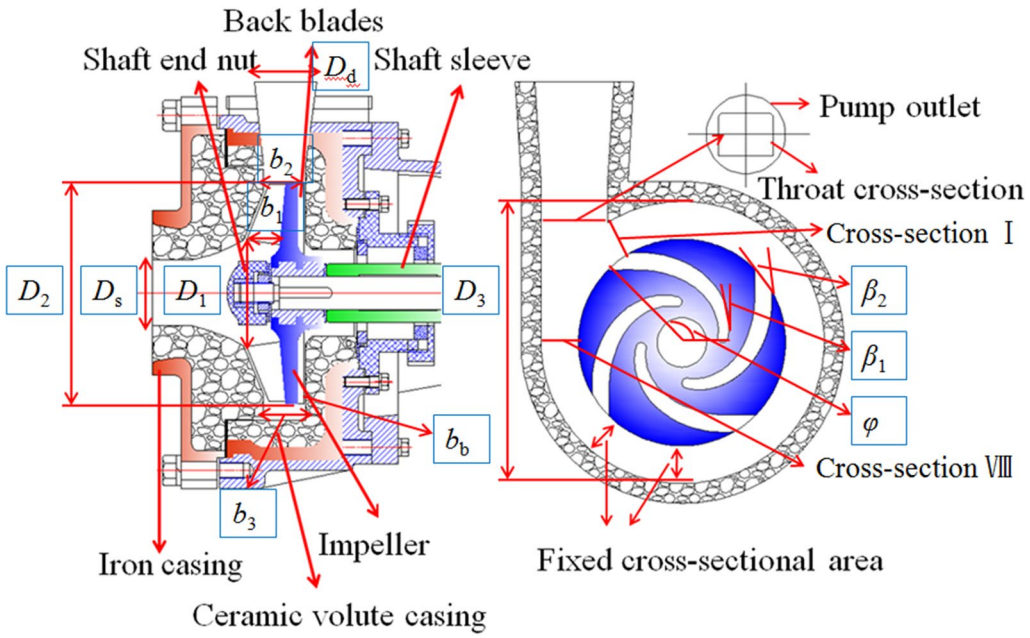

Figure 1 Pump structure

However, a significant portion of the flow will reenter the volute instead of being discharged to the outlet duct because of the large gap between the tongue and impeller that will decrease the pump performance [19]. Barrio et al. [20] reported the unsteady flow behavior close to the tongue region of a single-suction volute-type centrifugal pump. They found that the pulsation in leakage through the impeller-tongue gap increased by 30% when the flow rate increased by 60% from the rated condition. Alemi et al. [21] and Yang et al. [22] reported the influence of cross-sectional shape on the hydraulic performance of a centrifugal pump and found that the circular cross sectional shape could provide a higher pump head and efficiency than trapezoidal and rectangle shapes. Bowerman et al. [23], Chan et al. [24], and Chang et al. [25] reported that reducing the cross-sectional area could offset the optimal efficiency point to a smaller flow rate condition and result in a steeper pressure fall at the pump outlet, specifically under large flow rate conditions.

As far as the authors are aware, only limited studies have been reported in open literature considering centrifugal pumps with annular volutes, although numerous studies have reported the transient characteristics of conventional spiral volute casings. In this study, the influence of the cross-sectional area of the annular volute of a ceramic centrifugal pump on the transient characteristics and the pump hydraulic performance are investigated. Two volute casings were custom-built to experimentally validate the numerical results. It is anticipated that this study will be of benefit in the design of ceramic slurry pumps.

2 Pump Geometry

The pump under study is a single-stage horizontal centrifugal ceramic pump with an annular volute casing. The pump structure is shown in Figure 1. The components that are directly exposed to slurry, including the impeller, the volute casing, the shaft sleeve, and the shaft end nut, are made of engineering ceramic. The ceramic volute casing was enclosed in an iron housing to make provision for an accidental failure. The rated working condition of the ceramic pump is a flow rate Q of 100 m^3/h and a rotational speed n of 2900 r/min. The impeller is semi-open, namely without a front shroud, and has four backward-curved blades and 12 backward-curved back blades outside the back shroud. As opposed to the spiral volute casing used in conventional centrifugal pumps, the annular volute casing has a fixed cross-sectional area and a greater gap between the tongue and impeller exit. The cross-sectional area of the annular volute casing of the original case was designed to be identical to cross section VIII of the spiral volute casing, as shown in Figure 1, based on the velocity coefficient method [26]. The primary geometric dimensions of the ceramic pump are presented in Table 1.

Table 1 Primary geometric dimensions

Parameter	Value
Suction branch diameter D_s (m)	0.1
Discharge branch diameter D_d (m)	0.08
Impeller eye diameter D_1 (m)	0.09
Impeller exit diameter D_2 (m)	0.21
Leading edge width b_1 (m)	0.041
Trailing edge width b_2 (m)	0.028
Leading edge blade angle β_1 (°)	20
Trailing edge blade angle β_2 (°)	26
Blade wrap angle φ (°)	120
Back blade width b_b (m)	0.005
Volute chamber width b_3 (m)	0.063
Diameter to volute tongue D_3	Varying

3 Numerical Method

3.1 Calculation Domain and Grid Generation

Three cases, with volute tongue diameters of 281 mm (case 1), 305 mm (case 2), and 329 mm (case 3), were numerically simulated. For all three cases, the calculation domain comprised six modules, namely the suction branch, impeller, front chamber, back chamber, back blades, and volute casing. The entire calculation domain was meshed by hexahedral-structured grids with the aim of high precision and rapid convergence by the ANSYS ICEM 14.5 software. All the grids that bordered on solid walls, specifically the blade surfaces and the volute tongue region, were refined for the treatment of the wall function, as shown in Figure 2. A grid independence analysis was performed at the rated working condition for case 1 to investigate the effect of grid number and refinement method on the simulation results. As presented in Table 2, it can be seen that when the grid number reaches 4.02 million, the variation in the pump

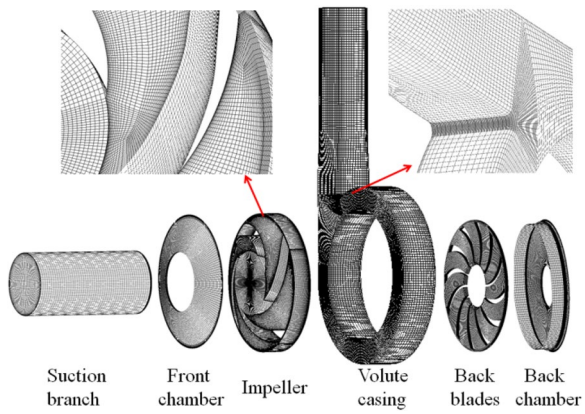

Figure 2 Calculation domain and grid meshing

Table 2 Grid independence analysis

Grid number	2071856	3115696	4021768	5013874
Head H (m)	47.38	48.02	48.43	48.61
Efficiency η (%)	59.26	59.87	60.22	60.49

performance is less than 1%. Therefore, a final cell number of 4021768 was utilized for case 1. Because there is no obvious structural difference between the three cases, the grid refinement and blocking method were used for the other two cases.

3.2 Pre-processing

The transient flow through the modeled pump was simulated using the commercial software ANSYS CFX 14.5, which utilized the finite volume method to solve the unsteady three-dimensional Navier–Stokes equations. Because of the fast convergence and the accurate hydraulic performance achieved compared to other turbulence models, the standard k-ε model was selected to complete the turbulence equation, with the standard wall function for the treatment of the flow in the boundary layer based on the refined grids [27]. All the solid walls in the computational domain were set as no-slip walls with a roughness of 0.2 mm. The surfaces of the impeller and back blades were set in a rotating reference frame with a rotational speed identical to the nominal operating speed of the pump [28, 29]. All the other surfaces were set in a stationary frame. The transient rotor–stator model was attached to the interfaces between the rotating and stationary regions. An axial velocity, based on the variation of the flow rate, was provided at the inlet boundary located at the suction branch. In addition, the outlet boundary was set as an opening with a specified static pressure in the case of the upstream influence of backflow on the primary flow domain. A high-resolution technique was used for the discretization of the advection scheme and turbulence terms. The second-order backward Euler method was applied for the transient scheme. The convergence criterion was set as 1×10^{-5} for the scaled residuals, with at least 20 iterations per time step. The time step was set as 0.000172414 s, as this provided a blade rotation of 3° between iterations, which means an impeller rotational period covers 120 time steps. Ten impeller revolutions were required when the flow reached a clear periodic regime. The data of one additional impeller revolution was then extracted to analyze the transient flow characteristics for each case. The data include the maximum, minimum, time-average, and standard deviation of the selected flow variables, including static pressure, total pressure, relative velocity, and absolute velocity.

4 Validation of CFD Results

To validate the capabilities of the numerical simulation, volute casings for case 1 and case 2 were manufactured for the hydraulic performance test. The test rig is an open type and comprises two pressure transducers with measurement errors of 0.25%, mounted at a short distance up and downstream of the pump inlet and outlet, a turbine flow meter with a measurement error of 0.5%, and a torque meter with a measurement error less than 0.1%. In addition, a valve is mounted at the outlet pipe to adjust the flow rate and a data acquisition instrument is used to record the parameters. The test rig processes the identification of a national grade 1 precision (GB/T 3216-2005) of the Department of Science and Technology in the Jiangsu province of China (Figure 3).

Figure 4 shows the comparison of the numerical and experimental *Q-H* and *Q-η* curves, showing a good quantitative agreement with the relative errors in heads smaller than 1.5%, and efficiency smaller than 3%, under the rated working condition. However, the difference between the simulation the test results increases when the flow rate offsets away from the rated working condition. Specifically, at a flow rate of 30 m^3/h, the difference in the head and efficiency were 4.8% and 8.2%, respectively. This is, in all probability, because of the limitation of the turbulence model in dealing with the significant vortex and backflow. In addition, the head curve of the case with the greater cross-sectional area exhibits a flat and rightward decreasing tendency overall, and the head curve of the case with the smaller cross-sectional area in the low flow rate region decreases slowly. It can be reasonably surmised that the small volute casing cross-sectional area could cause a hump in the pump head curve, which will result in a surge in the pipe system. At the rated working condition, the hydraulic performance

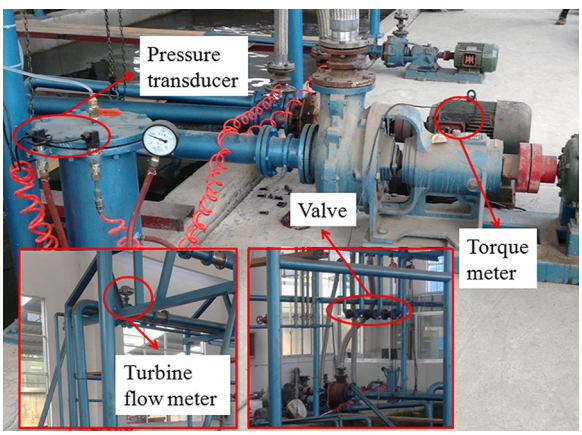

Figure 3 Test rig

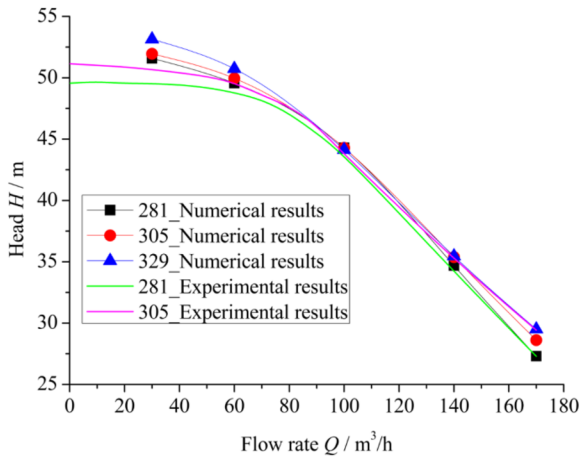

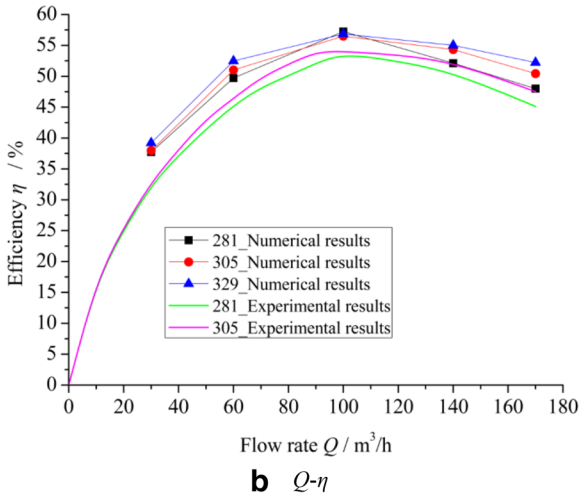

Figure 4 Comparison of numerical and experimental results

decreases marginally with increasing volute casing flow area. While the pump operation offsets away from the rated working condition, the case with a greater volute casing flow area exhibits improved hydraulic performance. In addition, the high-efficiency region widens with increasing volute casing flow area. In summary, from the comparisons it can be concluded that the numerical simulation can be considered adequate to investigate the unsteady flow behavior in the pump.

5 Results and Discussion

5.1 Hydraulic Loss in Volute Casing

Figure 5 shows the hydraulic loss in the annular volute casing for each case under five flow rates. It can be seen that the hydraulic loss in the volute casing is a maximum at the working condition for all three cases. The hydraulic loss increases with increasing volute flow rate at the working condition. However, the opposite can be

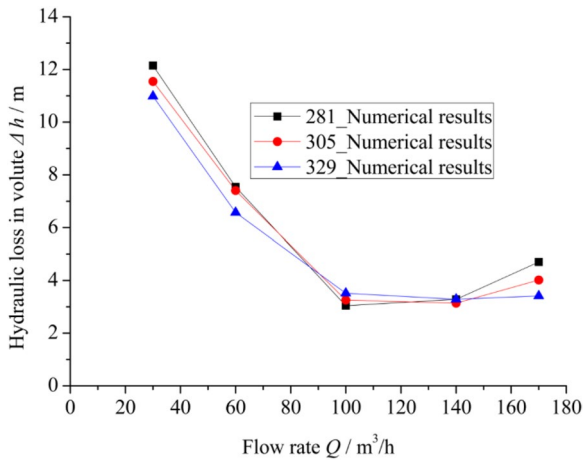

Figure 5 Hydraulic loss in volute casing

observed under large and small flow condition. As can be seen in Figure 4, the variation in pump performance at the working condition was less affected by the increases in the flow area. However, the hydraulic loss of the small volute casing flow area increases significantly under large and small flow condition. Typically, the greater hydraulic loss in the volute casing and impeller is the primary reason for the decrease in the pump head and efficiency. The variation in pump performance with increasing volute casing exhibits the same tendency with the change in hydraulic loss in the volute. Therefore, it can be concluded that the variation in the pump performance with the change in the volute casing flow area is primarily caused by the hydraulic loss in the volute casing. Detail regarding the flow variation in the volute casing with the change in the volute casing flow area will be discussed in the following section.

5.2 Analysis of Flow Rate Distribution at Cross-Sections

Figure 6 shows the flow rate at the cross sections of the annular volute under three working conditions with flow rates of 30 m^3/h, 100 m^3/h, and 170 m^3/h. It should be noted that cross section I (Figure 1) is located at 3° backward of the volute tongue. The other seven cross-sections have an equivalent deviation angle of 60°. Cross section 9 represents the throat cross section and cross section 11 the outlet of the pump. It can be seen that the flow rate increases from cross section I to cross section VIII regardless of the flow rate variation for all three cases. In addition, the increase in flow rate from cross section I to the throat cross section increases with increasing flow rate at the pump inlet. The flow rate at cross section I comprises two parts that can be observed in Figure 7. One part is the flow discharged from the impeller, and the other part is the flow from cross section VIII that flows back into the volute casing through the gap between the volute tongue and impeller periphery. When the pump operates at the low flow condition with a flow rate of 30 m^3/h, the bulk of the fluid circulates in the volute casing, as can be seen in Figure 7(a). Backflow occurs in the diffuser because of the significant pressure gradient and circulating flow. When the pump operates under the large flow condition with a flow rate of 170 m^3/h, the flow rate through the cross section I decreases significantly, as can be seen in Figure 6(c). The backflow occurs at positions backward from cross section I. In addition, it can be seen that the flow rate through cross section VIII is smaller than the pump flow rate. Therefore, a part of the fluid discharged from the impeller passage close to the volute tongue flows toward the throat cross section, resulting in the backflow, which can be seen in Figure 7(c). By comparing the flow rates of the three cases at the volute cross-sections, it can be observed that the increase in the volute flow area can increase the volute

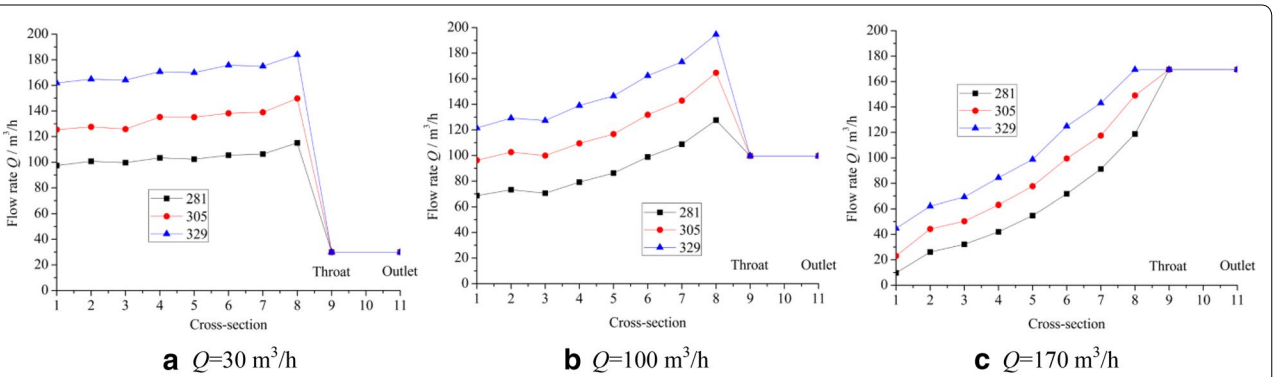

Figure 6 Hydraulic loss in volute casing

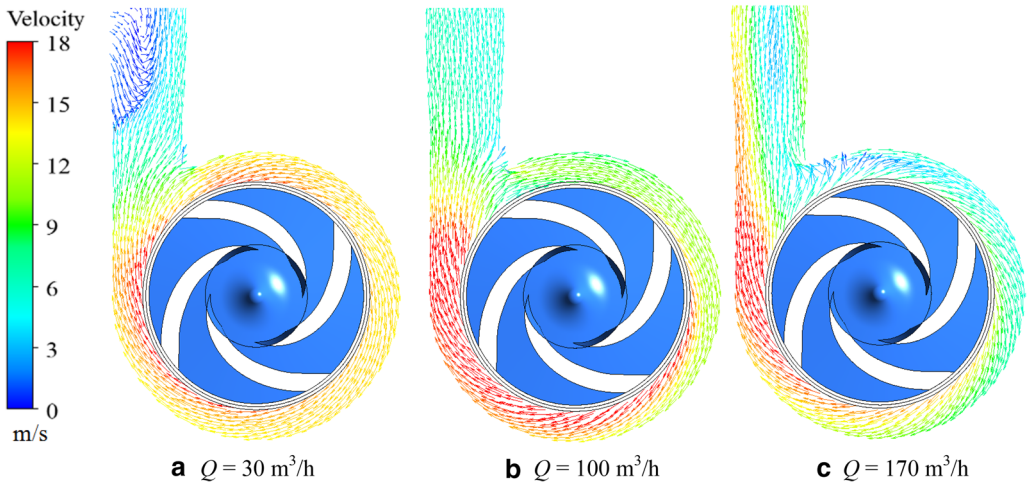

Figure 7 Velocity distribution at mid span of volute casing for case 1

flow capacity, which accordingly shifts the maximum efficiency point offsets toward the large flow condition.

5.3 Pressure and Velocity Distribution in Volute Casing

Figure 8 shows the distribution of static pressure and velocity at the volute casing inlet and the total pressure at the cross sections at the nominal flow rate for the three cases. It should be noted that the velocity, the static pressure, and the total pressure are time-averaged during one impeller revolution and can be extracted from the ANSYS CFX-Post software. As the flow rate increases from cross section I to cross section VIII, the velocity also increases. After the fluid flows through the cross section VIII, it will separate into two parts, one of which flows toward the throat cross section, and the other back into the volute through cross section I. Therefore, in Figure 8(a), it can be seen that the velocity decreases significantly from cross section VIII to cross section I and, in Figure 8(b), it can be seen that the static pressure clearly increases from cross section VIII to cross section I. By comparing the three cases, it can be observed that the static pressure becomes less uniform as the volute casing flow area decreases, specifically in the region close to cross section VIII. As can be seen in Figure 8(c), when the volute casing flow area increases, the total pressure from cross section I to cross section V increases, while the total pressure from cross section V to the pump outlet decreases. Typically, two symmetrical vortexes are anticipated at the cross section to achieve an improved hydraulic performance. As can be seen in Figure 9, the smaller flow area of the cross section results in additional asymmetric vortices at cross section I, which result in a lower total pressure. However, the area of the vortices at cross section VIII decreases with decreasing cross-sectional flow area, which results in a higher total pressure at cross section VIII. The vortices at the throat cross section for all the three cases are approximately identical, as is the decrease ratio of the total pressure from the throat cross section to the pump outlet. It can be observed that the vortex structure at cross section VIII has a greater effect on the hydraulic loss in the volute casing than the uniformity of the static pressure distribution at the volute casing inlet under the rated working condition.

Figure 10 shows the distribution of static pressure and velocity at the volute casing inlet, and the total pressure at cross-sections, at a flow rate of 30 m^3/h for the three cases. By comparing Figure 10(a) and Figure 8(a), it can be observed that the velocity from cross section I to cross section IV increases even with a decrease in the pump flow rate. The reason for this can be seen in Figure 6. Although the flow rate of pump decreases, the flow at cross section VIII remains approximately constant. Only the flow rate at the throat cross section decreases significantly, and the bulk of the fluid circulates in the volute through cross section I, as can be seen in Figure 7, resulting in the velocity in the volute increasing even though the pump flow rate decreases. Because the bulk of the fluid circulates in the volute, the static pressure gradient from cross section VIII to cross section I decreases with decreasing pump flow rate. By comparing the three cases, it can be observed that the static pressure remains increasing and the circumferential distribution of static pressure at the volute casing inlet becomes more uniform with the increase in the volute casing flow area, similar to the nominal flow rate condition. In addition, the total pressure increases as a whole with increasing casing flow area. As shown in Figure 11, there is only one vortex at cross section I and the area of the vortex decreases with

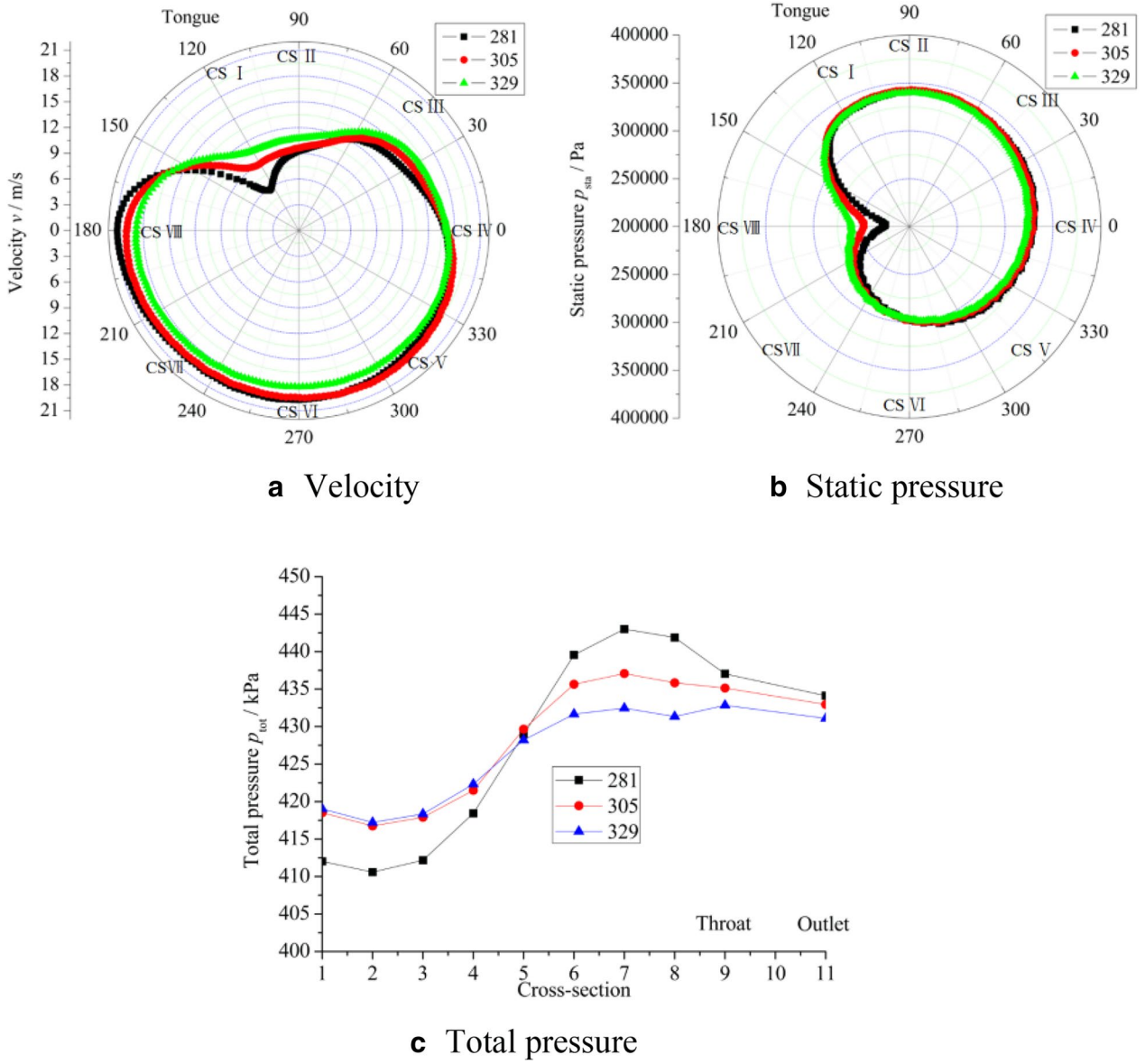

a Velocity **b** Static pressure

c Total pressure

Figure 8 Distribution of pressure and velocity in volute casing at nominal flow rate

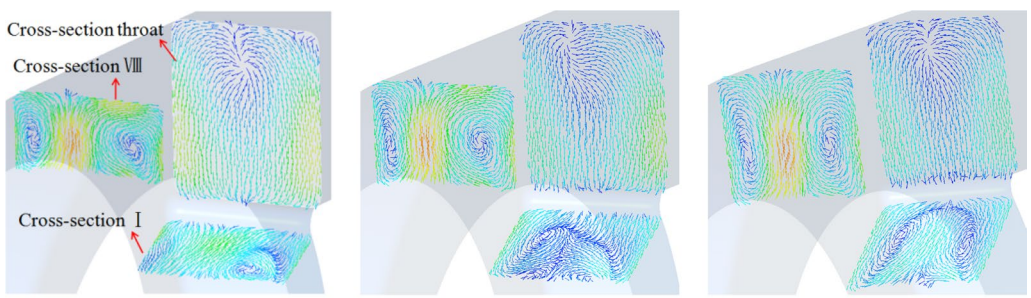

a Case 1: D_3=281 mm **b** Case 2: D_3=305 mm **c** Case 3: D_3=329 mm

Figure 9 Tangential components of velocity at cross-sections at nominal flow rate

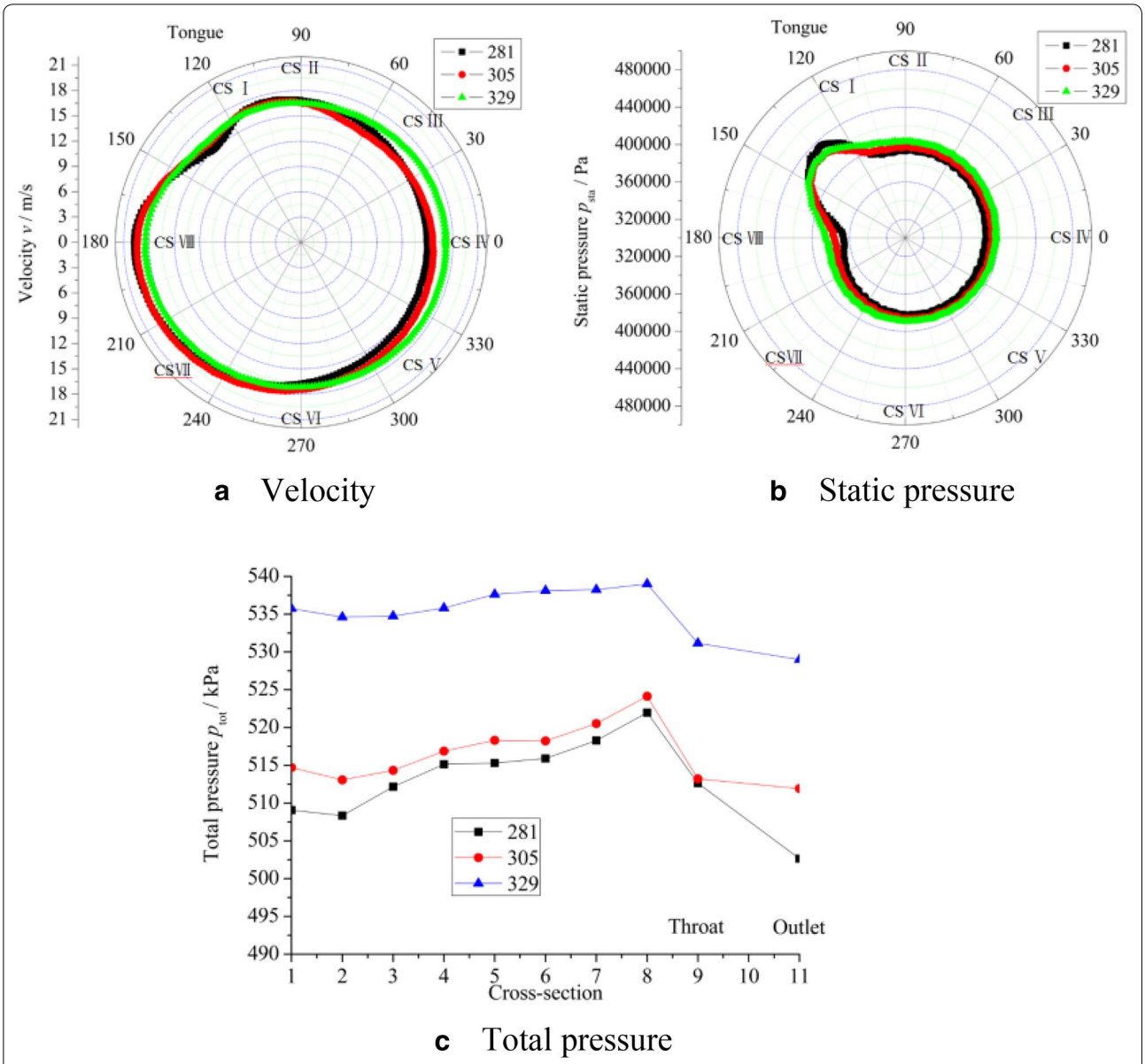

Figure 10 Distribution of pressure and velocity in volute casing at flow rate of 30 m^3/h

increasing volute casing flow area. Two asymmetric vortices can be observed at the throat cross section for all the three cases because the flow rate offsets at a distance from the designed point. The area of the left vortex decreases with increasing volute casing flow area. Under the effect of the nonuniform circumferential static pressure distribution at the volute casing inlet and the vortex structure at the cross sections, the volute with a greater flow area has a better hydraulic performance under the small flow condition.

Figure 12 shows the distribution of static pressure and velocity at the volute casing inlet, and the total pressure at the cross-sections, at a flow rate of 170 m^3/h for the three cases. It can be seen that the velocity distribution at the volute inlet in the flow direction exhibits a significant gradient, especially from cross section VIII to cross section I. The reason, as can be seen in Figure 6, is that the bulk of the fluid enters the diffuser through the throat cross section instead of circulating in the volute because of the large pump flow rate. The greater volute flow area results in a greater fluid capacity, which will decrease the velocity in the volute, especially the velocity at cross section VIII. The lower velocity at cross section VIII results in a smaller velocity gradient from cross section VIII to

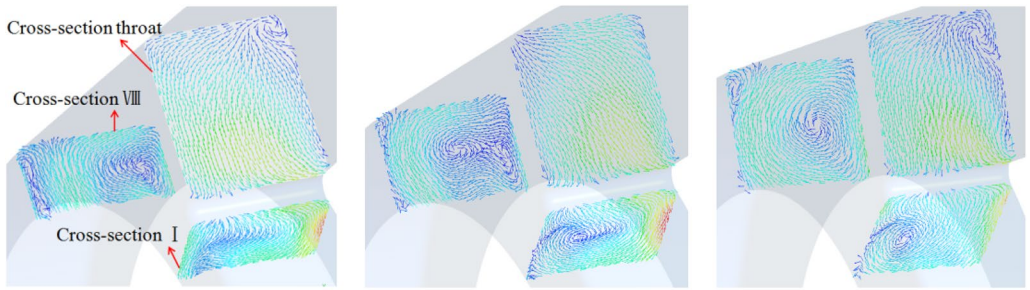

a Case 1: D_3=281 mm **b** Case 2: D_3=305 mm **c** Case 3: D_3=329 mm

Figure 11 Tangential components of velocity at cross-sections at flow rate of 30 m^3/h

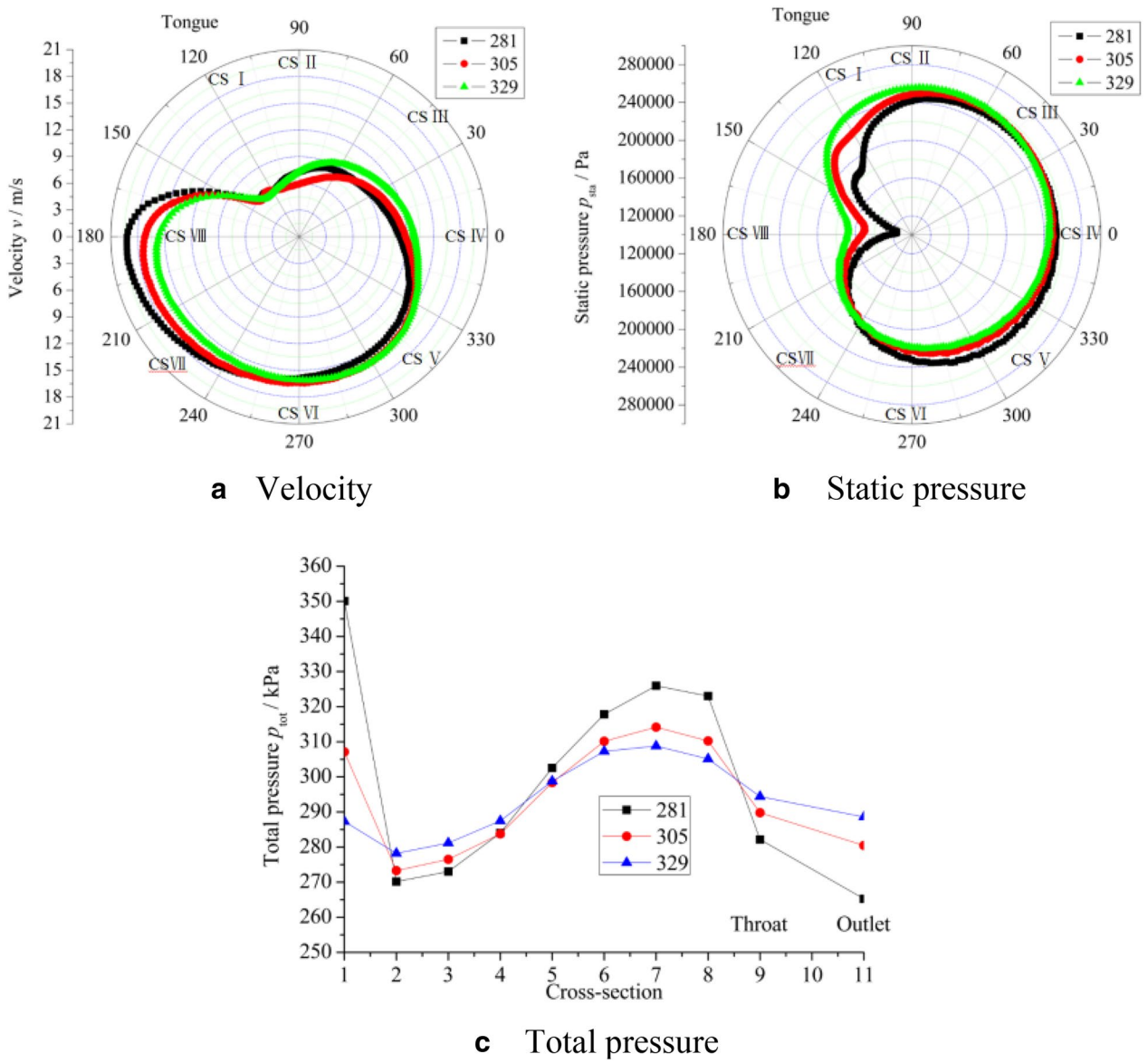

a Velocity **b** Static pressure

c Total pressure

Figure 12 Distribution of pressure and velocity in volute casing at flow rate of 170 m^3/h

cross section I, which results in a smaller static pressure gradient. As discussed above, the total pressure at cross section I decreases with increasing volute casing flow area. The reason has been analyzed before. The high-energy flow discharged from the impeller passage close to the volute tongue flows toward the throat cross section to supplement the flow rate, resulting in a greater total pressure in cross section I. Because of the lack of fluid flow into the volute casing, the total pressure from cross section II to cross section V decreases with increasing volute casing flow area. However, the total pressure decreases more sharply from cross section VII to the throat cross section because of the greater velocity gradient for the volute with the smaller flow area. As can be seen in Figure 13, the vortex structure at the cross-sections are approximately identical. Therefore, the backflow at cross section I and the significant velocity gradient from cross section VIII to the throat cross section are the primary reasons for the poorer hydraulic performance of the volute with the smaller flow area.

5.4 Pressure Pulsations in Annular Volute

To analyze the pressure pulsation, the dynamic pressure at the impeller periphery was used to present the pressure pulsations in a normalized form to allow the scaling of pressure pulsation data with respect to size and speed. The pressure pulsation coefficient C_p is defined as:

$$C_p = \frac{p - \bar{p}}{0.5\rho u_2^2}, \tag{1}$$

where $\bar{p}$ represents the time-averaged static pressure during the last impeller periods for each node, and u_2 is the circumferential component of the absolute velocity at the impeller periphery.

In addition, a non-dimensional pressure fluctuation intensity coefficient C_p^* was defined to determine the magnitude of the pressure fluctuations for an entire revolution period as follows:

$$C_p^* = \frac{1}{N}\sum_{i=0}^{N-1}\frac{\sqrt{(p(t_0 + i\Delta t) - \bar{p})^2}}{0.5\rho u_2^2}, \tag{2}$$

where t_0 represents the starting time for one impeller period of the transient simulation, and N is the sample number during the last revolution period.

Figure 14 shows the distribution of the fluctuation intensity coefficient as polylines in the annular volute. It can be seen that the coefficient increases as a whole with increasing flow rate for all the three cases. In addition, the polylines all exhibit four peaks, which is in accordance with the number of impeller blades. The four peaks have equivalent deviation angles of 90°. The greatest pressure pulsation occurs approximately 30° backward of the volute tongue, which means that the interaction between the impeller trailing edges and the volute tongue is the primary reason for the pressure pulsations in the volute. In addition, the increase in the volute flow area will alleviate the pressure pulsations in the volute regardless of the pump working condition.

5.5 Radial Force

To evaluate the pump vibration, the radial force on the shaft for the three cases was determined and the results are presented in Figure 15. It can be seen that the magnitude of radial force on the shaft increases with increasing pump flow rate. The radial force distribution appears as a quadrangle, which is in accordance with the impeller blade angles. In addition, the quadrangle rotates clockwise as the flow rate increases. The increase in the volute flow area can decrease the magnitude of the radial force on the shaft, specifically at the nominal flow rate and large flow condition that can decrease the pump vibration, which resulted in an improved operational stability of pump.

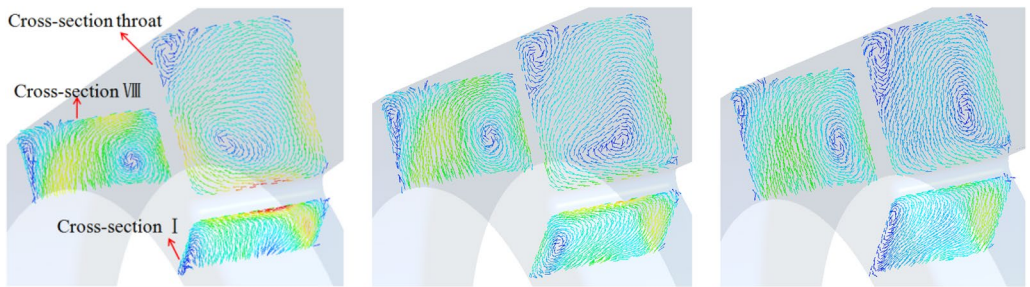

a Case 1: D_3=281 mm **b** Case 2: D_3=305 mm **c** Case 3: D_3=329 mm

Figure 13 Tangential components of velocity at cross-sections at flow rate of 170 m^3/h

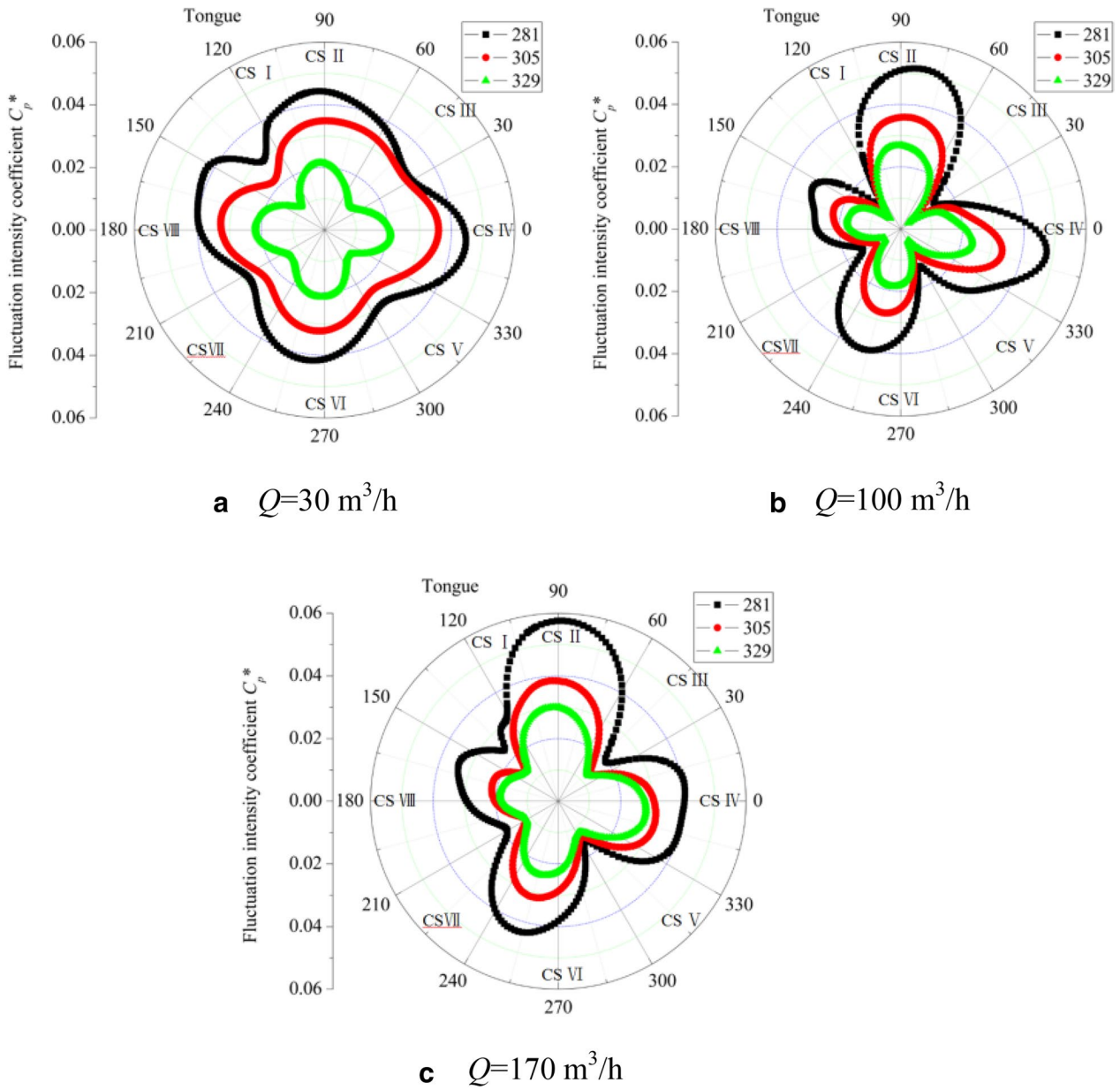

Figure 14 Distribution of fluctuation intensity coefficient at volute casing inlet

6 Conclusions

In this study, the influence of cross-sectional flow area of an annular volute on the hydraulic loss, pressure pulsations, and radial force on the shaft under varying working conditions in a centrifugal ceramic pump were investigated. Experiments were conducted for the validation of the numerical results. The primary conclusions were as follows.

(1) When the volute casing flow area increased, the hydraulic performance decreased marginally at the rated working condition but increased at off-design points, specifically under the large flow condition. However, the volute casing with a larger flow area had a wider high-efficiency region.

(2) The nonuniform circumferential static pressure distribution at the volute casing inlet and the vortex structure at the cross-sections were the primary reasons for the hydraulic loss in the volute under the rated and small flow conditions. However, for the large flow condition, the backflow at cross section I and the large velocity gradient from cross sec-

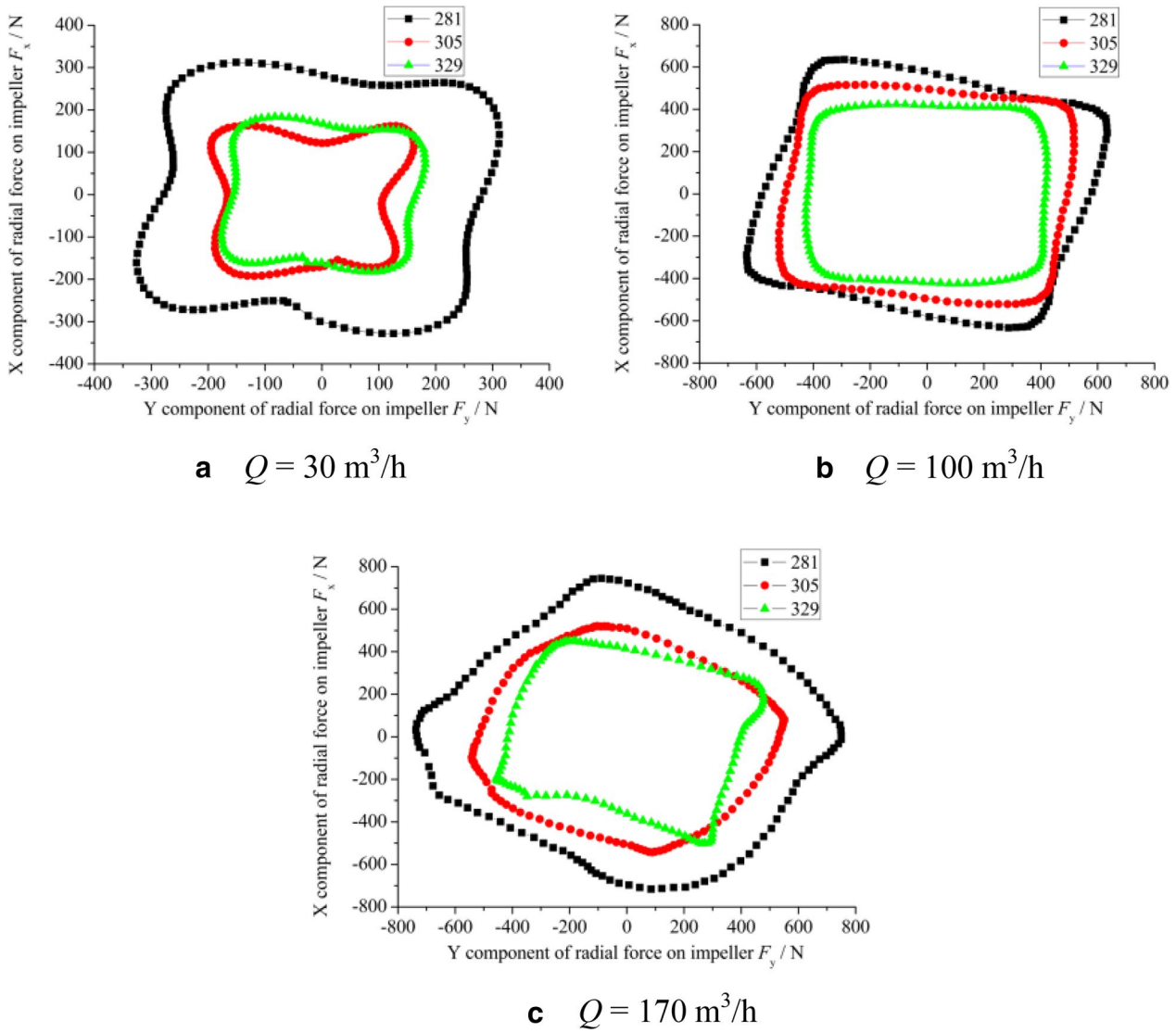

Figure 15 Radial force on shaft for three cases with flow rate variations

tion VIII to the throat cross section were the primary reasons.

(3) The greatest pressure pulsation occurred approximately 30° backward of the volute tongue. An increase in the volute flow area decreased the pressure pulsations in the volute regardless of the working condition, and decreased the radial force on the shaft, which resulted in an improved operational stability of pump.

It is anticipated that this study would be of benefit during the design of annular volutes. The annular volute cross-sectional area should be appropriately greater than cross section VIII of the spiral volute casing to achieve an improved hydraulic performance under large flow condition and an improved pump operational stability. However, it should be noted that a greater annular volute cross-sectional area will require a larger pump, which will increase material costs and make transportation more logistically difficult. Therefore, the cross-sectional area of the annular volute should be comprehensively considered during the design.

Authors' Contributions

YT was in charge of the whole trial; YT wrote the manuscript; SY, JL, and FZ assisted with sampling and laboratory analyses. All authors read and approved the final manuscript.

Author Details
[1] Wuxi Vocational Institute of Arts and Technology, Wuxi 214206, China.
[2] National Research Center of Pumps and System Engineering and Technology, Jiangsu University, Zhenjiang 212013, China.

Authors' Information
Yi Tao, born in 1988, is currently a lecturer at *Wuxi Vocational Institute of Arts and Technology, China.* He received his PhD degree from *National Research Center of Pumps and System Engineering and Technology, Jiangsu University, China*. His research interests include solid–liquid two-phase flow and design of slurry pumps.

Shouqi Yuan, born in 1963, is currently a professor and a PhD candidate supervisor at *National Research Center of Pumps and System Engineering and Technology, Jiangsu University, China*. He has received 16 prizes for science and technology advancement at province or ministry level. He has published 3 books and more than 240 papers. His research interests include the theory, design and CFD of pumps and fluid machinery.

Jianrui Liu, born in 1952, is currently a professor and a PhD candidate supervisor at *National Research Center of Pumps and System Engineering and Technology, Jiangsu University, China*. His research interests include fluid machinery engineering

Fan Zhang, born in 1987, is currently a PhD at *National Research Center of Pumps and System Engineering and Technology, Jiangsu University, China*. His research interests include flow characteristics in fluid machinery.

Competing Interests
The authors declare no competing financial interests.

Funding
Supported by National Natural Science Foundation of China (Grant No. 51779107), Jiangsu Provincial Natural Science Foundation of China (Grant No. BK20170548), Postdoctoral Science Foundation of China (Grant No. 2017M611724), and Priority Academic Program Development of Jiangsu Higher Education Institutions (PAPD).

Publisher's Note

Received: 8 May 2017 Accepted: 10 January 2019
Published online: 29 January 2019

References
[1] V V Burenin. Ceramic centrifugal pumps for the chemical and petroleum industries. *Chemical and Petroleum Engineering*, 2002, 38(7): 472–475.
[2] Y Tao, S Q Yuan, J F Zhang, et al. Numerical simulation and test on impeller wear of slurry pump. *Transactions of the Chinese Society of Agricultural Engineering (Transactions of the CSAE)*, 2014, 30(21): 63–69. (in Chinese)
[3] S Q Yuan, Y Tao, W D Cao, et al. 3D numerical simulation of internal flow in NTB multi-stage ceramic pump. *Journal of Drainage and Irrigation Machinery Engineering*, 2013, 31(10): 829–834. (in Chinese)
[4] Y Tao, S Q Yuan, J R Liu, et al. Numerical simulation and test research on the wear of back blades in slurry pumps. *ASME 2016 Fluids Engineering Division Summer Meeting*, Washington D C, USA, 2016.
[5] C I Walker. Slurry pump side-liner wear: comparison of some laboratory and field results. *Wear*, 2001, 250(2001): 81–87.
[6] P Li, Q Cai, B Wei. Failure analysis of the impeller of slurry pump used in zinc hydrometallurgy process. *Engineering Failure Analysis*, 2006, 13(6): 876–885.
[7] C E Brennen. Hydrodynamics of pumps. New York: Oxford University Press, 1994.
[8] Y Tao, S Q Yuan, J R Liu, et al. The influence of the blade thickness on the pressure pulsations in a ceramic centrifugal slurry pump with annular volute. *Proceedings of the Institution of Mechanical Engineers, Part A: Journal of Power and Energy*, 2017, 231(5): 415–431.
[9] B Neumann. The interaction between geometry and performance of a centrifugal pump. London: Mechanical Engineering Publications Limited, 1991.
[10] T Engin, M Gur. Performance characteristics of a centrifugal pump impeller with running tip clearance pumping solid-liquid mixtures. *Journal of Fluids Engineering*, 2001, 123(3): 532–538.
[11] A A Noon, M H Kim. Erosion wear on centrifugal pump casing due to slurry flow. *Wear*, 2016, s364-365(2016): 103–111.
[12] R Tarodiya, B K Gandhi. Hydraulic performance and erosive wear of centrifugal slurry pumps – A review. *Powder Technology*, 2017, 305(2017): 27–38.
[13] J R Kadambi, P Charoenngam, A Subramanian, et al. Investigations of particle velocities in a slurry pump using PIV: Part 1, the tongue and adjacent channel flow. *ASME Journal of Energy Resources Technology*, 2004, 126(12): 271–278.
[14] M F Khalil, S Z Kassab, A A Naby, et al. Performance characteristics of centrifugal pump conveying soft slurry. *American Journal of Mechanical Engineering*, 2013, 1(5): 103–112.
[15] Y Zhong, K Minemura. Measurement of erosion due to particle impingement and numerical prediction of wear in pump casing. *Wear*, 1996, 199(1): 36–44.
[16] J L Parrondo, J González, J Fernández. The effect of operating point on the pressure fluctuations at the blade passage frequency in the volute of a centrifugal pump. *ASME Journal of Fluids Engineering*, 2002, 124(3): 784–790.
[17] R Spence, J Amaral-Teixeira. A CFD parametric study of geometrical variations on the pressure pulsations and performance characteristics of a centrifugal pump. *Computers & Fluids*, 2009, 38(6): 1243–1257.
[18] H Alemi, S A Nourbakhsh, M Raisee, et al. Effect of the volute tongue profile on the performance of a low specific speed centrifugal pump. *Proceedings of the Institution of Mechanical Engineers, Part A: Journal of Power & Energy*, 2015, 229(2): 210–220.
[19] J C Cai, J Pan, A Guzzomi. The flow field in a centrifugal pump with a large tongue gap and back blades. *Journal of Mechanical Science and Technology*, 2014, 28(11): 4455–4464.
[20] R Barrio, J Parrondo, E Blanco. Numerical analysis of the unsteady flow in the near-tongue region in a volute-type centrifugal pump for different operating points. *Computers & Fluids*, 2010, 39(5): 859–870.
[21] H Alemi, S A Nourbakhsh, M Raisee, et al. Effects of volute curvature on performance of a low specific-speed centrifugal pump at design and off-design conditions. *ASME Journal of Turbomachinery*, 2015, 137(4): 041009.
[22] S S Yang, F Y Kong, B Chen. Research on pump volute design method using CFD. *International Journal of Rotating Machinery*, 2011, 2011(2): 1–7.
[23] R D Bowerman, A J Acosta. Effect of the volute on performance of a centrifugal pump impeller. *Transaction of the ASME*, 1957, 79(5): 1057–1069.
[24] W K Chan, Y W Wong, W Hu. Design considerations of volute geometry of a centrifugal blood pump. *Artificial Organs*, 2006, 29(12): 937–948.
[25] H S Chang, H B Jin, M J Kom, et al. Spiral casing of a volute centrifugal pump. *Journal of Mechanical Science and Technology*, 2014, 28(7): 2697–2706.
[26] X F Guan. *Modern pumps theory and design*. Beijing: China Astronautic Publishing House, 2011.
[27] I Chalghoum, H Kanfoudi, S Elaoud, et al. Numerical modeling of the flow inside a centrifugal pump: influence of impeller-volute interaction on velocity and pressure fields. *Arabian Journal for Science & Engineering*, 2016, 41(11): 4463–4476.
[28] W Dong, W L Chu. Numerical analysis and validation of fluid pressure in the back chamber of centrifugal pump. *Journal of Mechanical Engineering*, 2016, 52(4): 165–170. (in Chinese)
[29] Z L Liu, S Zhang, A C Shao, et al. Theoretical computation and verification for fluid static pressure in centrifugal pump side chamber. *Journal of Mechanical Engineering*, 2016, 52(4): 178–184. (in Chinese)